



OPEN ACCESS

EDITED BY

Tao Hu,
China University of Petroleum, Beijing, China

REVIEWED BY

Umar Ashraf,
Yunnan University, China
Amr S. Zaky,
Menoufia University, Egypt

*CORRESPONDENCE

Jingchun Tian,
✉ tjc@cdupt.edu.cn

RECEIVED 19 January 2025

ACCEPTED 03 February 2025

PUBLISHED 03 March 2025

CITATION

Jing X, Tian J, Zhang L, Li F and Li H (2025)
Dolomitization of Ordovician Kelimoli
carbonates linking to shale oil formation,
western Ordos Basin: new insights from
magnesium and strontium isotopes.
Front. Earth Sci. 13:1563155.
doi: 10.3389/feart.2025.1563155

COPYRIGHT

© 2025 Jing, Tian, Zhang, Li and Li. This is an
open-access article distributed under the
terms of the [Creative Commons Attribution
License \(CC BY\)](https://creativecommons.org/licenses/by/4.0/). The use, distribution or
reproduction in other forums is permitted,
provided the original author(s) and the
copyright owner(s) are credited and that the
original publication in this journal is cited, in
accordance with accepted academic practice.
No use, distribution or reproduction is
permitted which does not comply with
these terms.

Dolomitization of Ordovician Kelimoli carbonates linking to shale oil formation, western Ordos Basin: new insights from magnesium and strontium isotopes

Xianghui Jing^{1,2,3}, Jingchun Tian^{1*}, Lei Zhang^{2,3}, Fengjie Li¹ and Han Li^{2,3}

¹Institute of Sedimentary Geology, Chengdu University of Technology, Chengdu, China, ²Exploration and Development Research Institute of Changqing Oilfield Company, PetroChina, Xi'an, China, ³National Engineering Laboratory of Exploration and Development of Low Permeability Oil and Gas Fields, Xi'an, China

Deciphering the dolomitization process has great significance for high-quality hydrocarbon reservoir prediction in carbonate successions. The Ordovician Wulalike Formation provides shale oil in the western Ordos Basin, while lateral-contact marine dolostones of Kelimoli Formation contribute major reservoirs for extra hydrocarbons. Nonetheless, the origin and occurrence of dolostones are underexplored. Coupled with petrographic and lithologic analyses, this study attempts to investigate the dolomitizing fluid pathways and dolomitization pattern of Ordovician Kelimoli carbonates based on elemental and isotopic geochemistry. Extremely low Rb concentrations (i.e., less than 0.1) and Mn/Sr ratios (i.e., less than 2) of carbonates with micropores indicated that they are a valid proxy for geochemical signatures of coeval seawater. By contrast, dolostones developing vuggy pores showed a pronouncedly higher ⁸⁷Sr/⁸⁶Sr composition and Mn contents than other dolostone types, revealing that vuggy dolostones experienced meteoric water leaching and underwent geochemical alterations. Quantitative calculation of ⁸⁷Sr/⁸⁶Sr ratios and fluid-inclusion microthermometry revealed that the Kelimoli dolostones (i.e., dolograinstones and crystallized dolostones) were formed before meteoric water leaching influences at a deep-burial environment under seawater derivatives and sealed brine water. In evaporite–dolograinstone successions, increase in the magnesium isotopic composition ($\delta^{26}\text{Mg}$) with increasing burial depths indicated that the dolomitizing fluid migrated downwardly. Comprehensive isotopic evidences of ⁸⁷Sr/⁸⁶Sr, $\delta^{18}\text{O}$, and $\delta^{13}\text{C}$ suggested that the dolomitizing fluid was a derivative of coeval seawater. In crystallized dolostone successions, upwardly heaving of $\delta^{26}\text{Mg}$ ratios revealed that the dolomitizing fluid moved upwardly. The ⁸⁷Sr/⁸⁶Sr, $\delta^{18}\text{O}$, and $\delta^{13}\text{C}$ and microthermometric evidence indicated that these dolostones were formed at a deep-burial, high-temperature environment and the dolomitizing fluid was derived from sealed brine water. Based on the above investigation, a

comprehensive dolomitizing pattern was proposed for the studied section of Ordovician Kelimoli Formation.

KEYWORDS

dolomitization, shale oil, magnesium isotopes, Kelimoli Formation, western Ordos Basin

1 Introduction

Dolostones compared to limestones contribute major hydrocarbon reservoirs in carbonate successions due to the developing higher porosity and permeability, particularly at deep-burial depths (Warren, 2000; Liu et al., 2016). Deciphering dolomitization is significant for high-quality reservoir prediction in carbonates. Multiple dolomitization processes, including evaporative pumping, seepage reflux, burial, hydrothermal, and microbial dolomitization, were proposed in previous studies (Davies and Smith, 2006; Azomani et al., 2013; Liu et al., 2016). However, the occurrence of massive dolomites characterized by a wide distribution or/and great thickness is controversial, particularly for origin and Mg^{2+} migration (e.g., the dolostones investigated in the current study, i.e., the Ordovician Kelimoli Fm. in western Ordos Basin). Recent studies revealed that high-resolution magnesium isotopes (i.e., $\delta^{26}Mg$) provided a new proxy for tracing the migration pathways of Mg-rich dolomitizing fluids (Bialik et al., 2018; Ning et al., 2020). During the dolomitizing process, light-Mg (i.e., ^{24}Mg) from dolomitizing fluids was incorporated preferentially into calcite lattices to replace Ca^{2+} and form dolomites. Hence, the dolomitizing fluids became gradually rich in ^{26}Mg . Meanwhile, the dolomites formed in these diagenetic fluids were characterized by high $\delta^{26}Mg$ composition as dolomitizing fluids migrated forward (Bialik et al., 2018; Li et al., 2019). Hence, variations in the $\delta^{26}Mg$ composition of dolomites can indicate migrating pathways of dolomitizing fluids. Nonetheless, the $\delta^{26}Mg$ composition of marine dolostones displayed no regular trend or had connection to geological events. Moreover, it showed no variable ranges with respect to dolomites of different origins in marine carbonates (Higgins et al., 2018; Kimmig et al., 2021). Therefore, the $\delta^{26}Mg$ composition is not applicable for chemostratigraphy analysis. Comprehensive isotopic (e.g., $^{87}Sr/^{86}Sr$, $\delta^{13}C$, and $\delta^{18}O$) and elemental (e.g., Mn, Sr, Fe, and rare-earth elements) geochemistry and lithology–petrography are important methods for $\delta^{26}Mg$ analysis in elucidating dolomite origin and occurrence (Murray et al., 1991; Webb and Kamber, 2000; Shields and Stille, 2001; Nothdurft et al., 2004; Webb et al., 2009; Liu et al., 2016; Liu et al., 2017).

Ordovician dolostones are shale oil-bearing rocks in the western margin of the Ordos Basin. The Kelimoli Fm. rocks are mainly bioclastic dolomites, dolarenites, and granular dolomites with an average porosity of 12%. It is laterally contacting with the Wulalike shale oil Formation and accepting hydrocarbon charging from it. Thus, the Kelimoli hydrocarbons are of the same source with the Wulalike shale oil (Hu et al., 2024a; Hu et al., 2024b). Based on lithofacies, petrography, and carbon and oxygen isotope analyses, different dolomitization patterns for Ordovician carbonates in the western margin of the Ordos Basin were proposed, including evaporative pumping, meteoric water–seawater

mixing, hydrothermal, and microbial dolomitizations (Hou et al., 2003; Wang et al., 2009; He et al., 2014; Wu et al., 2020). Particularly, the meteoric water–seawater mixing dolomitization prevailed because meteoric water leaching was widely observed in Ordovician dolostones (Su et al., 2016). However, the origin and occurrence of these massive dolomites were controversial. In this study, magnesium ($\delta^{26}Mg$) and strontium ($^{87}Sr/^{86}Sr$) isotopes, coupled with carbon ($\delta^{13}C$) and oxygen ($\delta^{18}O$) isotopes, trace elements, and fluid inclusions, were investigated to determine the origin and occurrence of massive dolomites from the Kelimoli Fm. The study of Kelimoli Formation features has important significance to understand the whole petroleum system sourced from the Wulalike shale oil. Moreover, this study provides a new insight for elucidating the origin and occurrence of dolomites from a similar geological setting and has significance for prediction of high-quality dolostone reservoirs in the western margin of the Ordos basin.

2 Geological setting

The Ordos Basin is a polycyclic craton basin. It is divided into six structural units according to its present-day tectonics, namely, the Yimeng uplift, the Xiyuan thrust, the Tianhuan depression, the Yi-Shan slope, the Jinxi flexural fold, and the Weibei uplift (Figure 1A). The studied area, i.e., the western Ordos Basin, mainly covered the Xiyuan thrust and the Tianhuan depression belts. The Ordovician carbonate succession in the western Ordos Basin is an important target for shale oil and gas exploration (Hu et al., 2025; Figure 1B). The sedimentation of the western Ordos Basin was jointly controlled by the evolution of the Helanshan aulacogen and expansion of the Qilianshan trough. During the early Ordovician Period (i.e., the Zhuozishan Period), the terrestrial–marine transitional tidal flat gradually evolved into a platform ramp with the expansion of the trough (Li, 2019; Yu et al., 2021). At the Kelimoli Period, the paleogeography evolved from a platform ramp into an open platform with the development of tension rifting and syn-depositional normal faulting at the western Ordos Basin. After the Middle Ordovician Period, the depositional environment changed into a deep-water slope gradually due to increasing water depths in the western part of the basin caused by uplifting and formation of the middle-eastern ancient continent (Yu et al., 2021; Figure 1C). During the Ordovician period, a set of stable carbonate successions with clastic interbeds was deposited in the western Ordos Basin. The Ordovician strata can be divided into five formations from old to new according to litho- and bio-stratigraphy, i.e., the Sandaokan Fm., the Zhuozishan Fm., the Kelimoli Fm., the Wulalike Fm., and the Lashizhong Fm. (Figure 1C). The Kelimoli Fm., a main gas exploration target in the western Ordos Basin, was dominantly composed by dolostones with an average thickness of 40 m (Yu et al.,

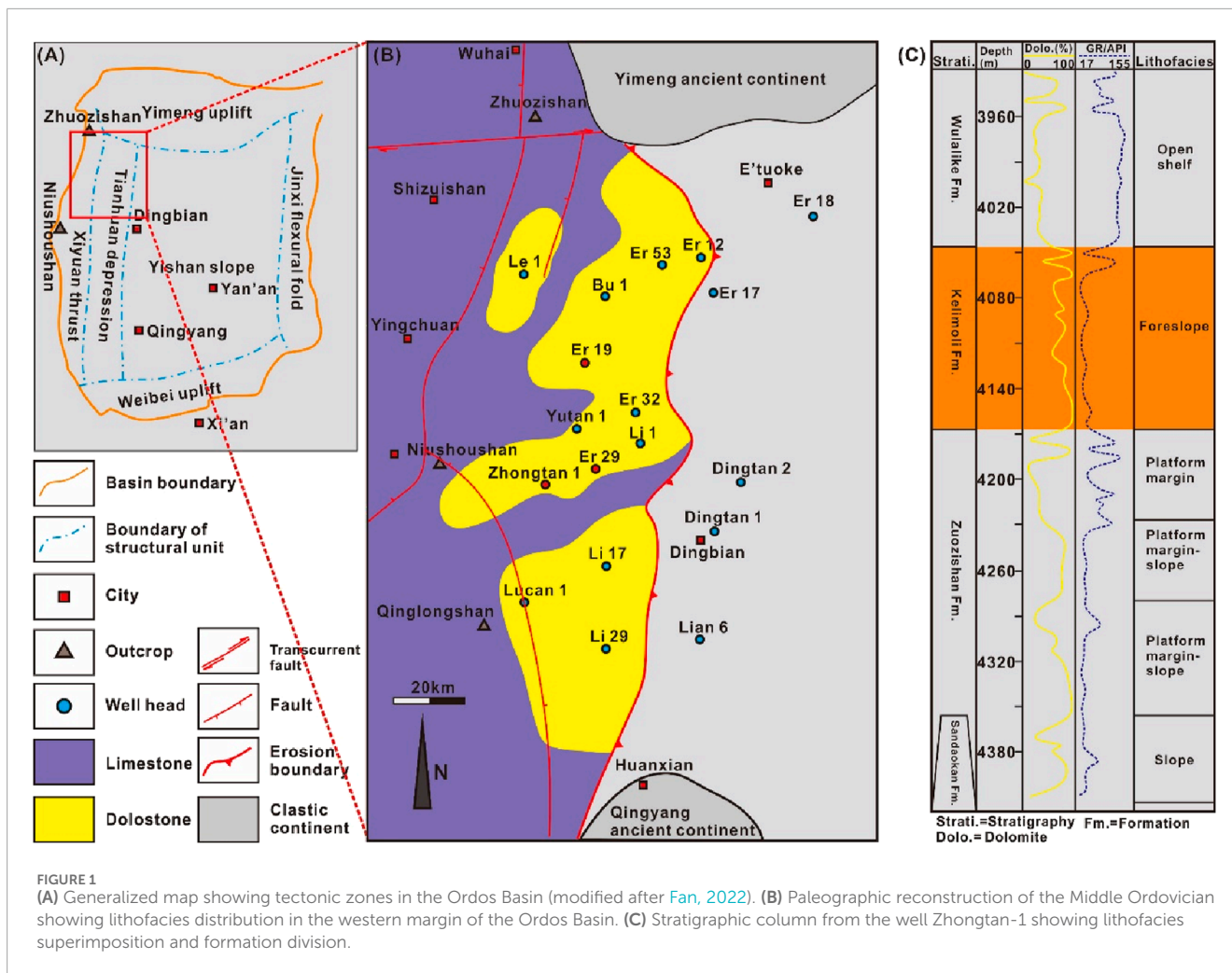


FIGURE 1 (A) Generalized map showing tectonic zones in the Ordos Basin (modified after Fan, 2022). (B) Paleographic reconstruction of the Middle Ordovician showing lithofacies distribution in the western margin of the Ordos Basin. (C) Stratigraphic column from the well Zhongtan-1 showing lithofacies superimposition and formation division.

2021) and limestone intercalations. The dolomites in the southern part of the western margin of the basin were mainly located in the lower part of the Kelimoli Fm., while the dolomites in the northern part mainly occurred in the upper part of the Kelimoli Fm. The Kelimoli dolostones were distributed continuously over an area of 8,000 km² (Figure 1B).

3 Samples and methods

Sixty-eight core samples with a total length of 23.65 m were collected from the Zhongtan-1, the Er-29, and the Er-19 wells. Twenty-three hand specimens were obtained from the Zhuozishan outcrop (well and outcrop locations are shown in Figure 1B). Full-length cores and hand specimens were studied at field for a general understanding of the lithology.

Thirty-three thin-sections stained with a mixed solution of potassium ferricyanide and Alizarin-S to differentiate calcites and dolomites were prepared for microscopic observation (Dickson, 1965). Meanwhile, all subsamples obtained from cores and hand specimens were crushed into particles finer than 80 meshes and then purified by distilled water and nitric acid solution (concentration of 65%). The dry powder was separated into four

aliquots for different measurements (referring to Ali et al., 2022; Ashraf et al., 2024a; Ashraf et al., 2024b).

X-ray fluorescence (XRF) analysis was undertaken on one aliquot of powdered samples to determine major elements. The powder samples were burnt to determine the loss of ignition (LOI). Subsequently, samples were compacted and smoothed for XRF measurement using a D3 Phaser spectrometer with an X1 ray tube as the excitation source. Measurement results were calibrated with the SiO₂ matrix at a detection time of 2 min, resulting in a testing error less than 2%.

Trace element (i.e., Rb, Sr, Fe, and Mn) contents were determined by an inductively coupled plasma mass spectrometer (ICP-MS). In addition, ~50-mg subsamples of another aliquot were prepared using the method given above. The treated samples were dried and then diluted with solution composed by 2 mL 1:1 HNO₃ and internal-standard solution (RhNO₃ concentration of 10 × 10⁻⁹ (wt)). Then, the prepared solution was sent for ICP-MS detection with an Agilent-7700e detector. Repeating examinations of standardized solutions of BHVO-1 (USGS) and EAV-56 (AGSO) showed that the measurement standard deviation (SD) was less than 0.03 × 10⁻⁶. Detailed procedures and parameter settings can be referred to Imai et al. (1996) and Liu et al. (2023).

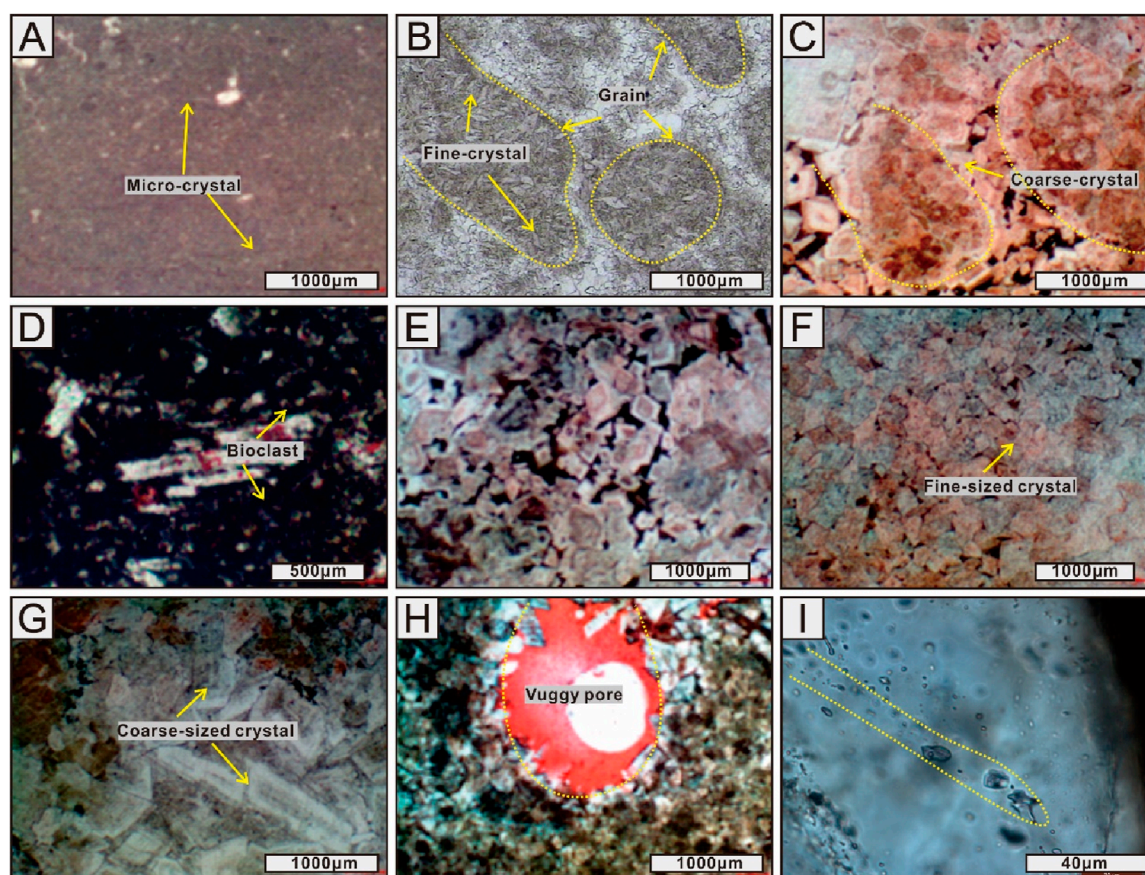


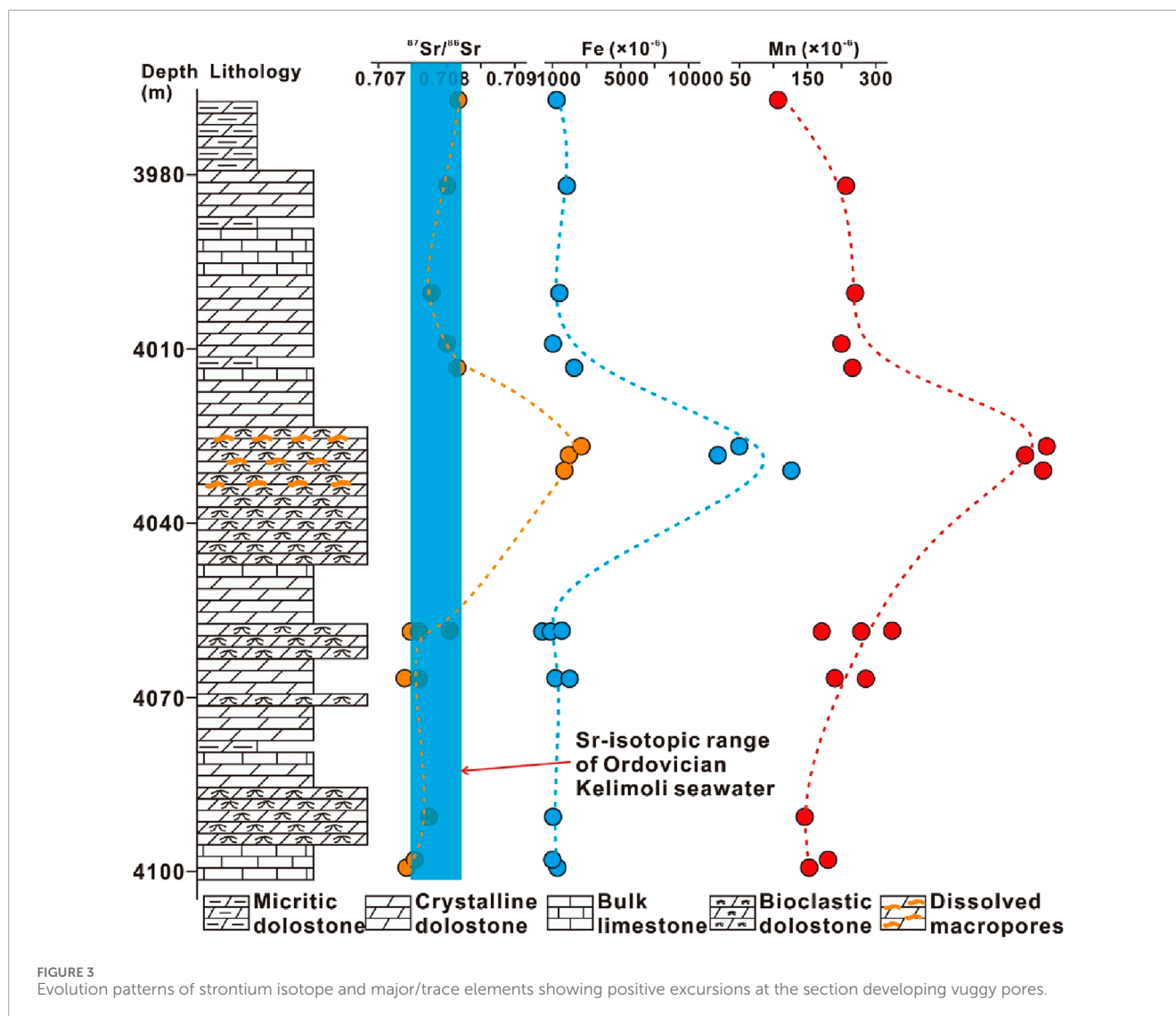
FIGURE 2

Photomicrographs showing lithofacies and mineralogy of carbonate samples from the Ordovician Kelimoli Fm. of the studied area under plane-polarized light (A, B, I) and cross-polarized light (C–H). (A) Evaporative shoals developing dolomites of micritic crystals. Well Zhongtan-1, 4018.64 m. (B) Dolograinstones developing dolomites of fine-sized crystals. Well Zhongtan-1, 4040.11 m. (C) Dolograinstones developing dolomites of medium- to coarse-sized crystals. Well Zhongtan-1, 4043.21 m. (D) Dolarenites developing bioclasts and bio-fossil debris. Well Er-29, 3885.67 m. (E) Cloudy-core–clear-rim texture being widespread in fine- to medium-crystallized dolomites. Well Er-29, 3915.91 m. (F) Crystalline dolomites developing fine-sized crystal assemblages. Well Er-19, 4110.51 m. (G) Crystallized dolomites developing clean, coarse crystals. Well Er-19, 4113.67 m. (H) Dolograinstones experienced meteoric-leaching dissolution, developing vuggy pores. Zhuozishan outcrop. (I) Dolomite crystals developing fluid-inclusion arrays. Zhuozishan outcrop.

For ^{13}C and ^{18}O isotopic determination, the powdered samples were treated with ultra-pure phosphoric acid at 100°C to produce carbon dioxide. Then, the CO_2 was analyzed using an MAT-253 mass spectrometer linked with Finnigan GasBench interface. The results were reported with the Vienna Pee Dee Belemnite (V-PDB) standard, and analytical precisions were 0.05‰ for $\delta^{13}\text{C}$ and 0.08‰ for $\delta^{18}\text{O}$. For $^{87}\text{Sr}/^{86}\text{Sr}$ determination, the powdered samples were dissolved in acidic solution composed by HF (3 mL) and HClO_4 (2 mL). Subsequently, the treated solution was sent for chemical separation of strontium using cation-exchange resin (AG 50 W*12, 200 meshes). Before conducting mass spectrometry, a standardized solution of NIST SRM 987 (concentration of 200 $\mu\text{g}/\text{L}$) was measured for parameter calibration. The sample solution containing strontium ions was introduced into the Neptune mass spectrometer with 2 (wt)% HNO_3 for measurement. Before conducting the measurement of another sample, the sample introduction system was cleaned with HNO_3 (3 (wt)%) to remove the memory effect. Detailed measurement

procedures and equipment parameters are given in *sensu* Yang et al. (2005). The result precision was better than 0.01‰ . The Mg-isotopic composition for dolomite samples was determined. The cation-exchange resin Bio-Rad AG50W-X8 (400 meshes) was used for chemical separation of Mg. The standardized sample of JD0-1 was used for parameter calibration. The measurement procedure was identical to that of $^{87}\text{Sr}/^{86}\text{Sr}$ composition. The result precision was of 0.08‰ according to the tracing measurement from the reference sample.

Fluid-inclusion microthermometry was conducted on dolomite samples. Doubly polished, 0.8-mm-thick thin-sections were prepared and then observed with an electronic microscope. Micro-areas developing fluid inclusion assemblages (FIAs) were marked and obtained by dissolving in acetone solution. Homogenization temperatures (T_h) were measured on primary liquid–vapor inclusions using a Linkam THMS-500 heating–freezing stage. Detailed measurement procedures followed the process described by Shepherd et al. (1985) and Liu et al. (2017).



4 Results

4.1 Petrofacies and mineralogy

Ordovician Kelimoli Fm. in the western Ordos Basin consists of limestone and dolostone petrofacies (Figure 1). Bulk limestones with textures ranging from micrites through wacke-/pack-stones to grainstones exhibited no reservoir potential. By contrast, high-potential reservoirs were developed in dolostone successions. Three dolomite types are recognized based on petrographic and mineralogic features (Amthor et al., 1993; Liu et al., 2017). The first type is distributed laminated, developing micritic crystals with sizes generally less than 10 μm with a nonplanar texture (Figure 2A). The second type is dolograinstones, including ooidic grainstones, bioclastic, and bioclastic-debris grainstones. Dolomites of variable crystal sizes (i.e., ranging from 20 μm to 100 μm) and biofossils are developed (Figures 2B–D). The crystal textures are mainly planar-s. The third type is crystalline dolomite characterized by fine- to coarse-sized crystals with sizes ranging from 30 μm to 200 μm (Figures 2E–G). The crystals show planar-e and planar-s

euhedral and cloudy-core-clear-rim texture (Figure 2E). Meanwhile, dolograinstones developed numerous vuggy pores with sizes larger than 1,000 μm (Figure 2H). In crystalline dolomites, linearly arrayed fluid-inclusions developed widely in dolomite crystals (Figure 2I).

4.2 Major and trace element characteristics

Major elements were analyzed from core samples. From limestones to dolostones, the content of MgO increased from 1.03% to 65.98% with a mean value of 35.57%. The mean content of TFe ($\text{Fe}_2\text{O}_3 + \text{FeO}$) from vuggy dolostones is 11.81%, pronouncedly higher than that in other types (ranging from 0.46% to 5.75% with mean value of 2.56%) and showing positive excursion at the corresponding section (Supplementary Table S1; Figure 3).

Trace elements, including Sr, Rb, and Mn, were analyzed. The Sr and Mn concentrations of vuggy dolostones and other carbonates (i.e., marl limestones, bioclastic limestones, crystalline dolostones, and dolograinstones) showed different values, ranging from 785×10^{-6} to $1,213 \times 10^{-6}$ of Mn (mean value of 1,041

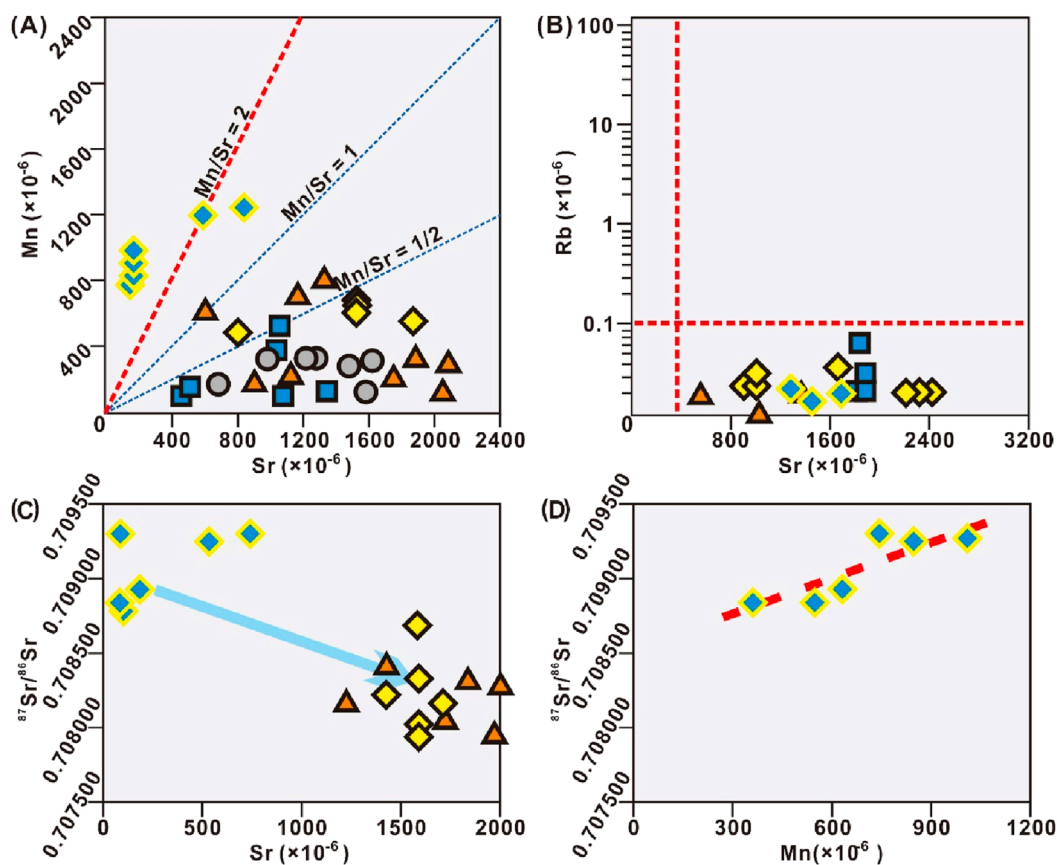


FIGURE 4

Crossplots showing trace element contents of carbonate samples from the studied interval. (A) Mn/Sr ratios vary from different carbonate samples. (B) Rb concentrations are exclusively lower than 0.1×10^{-6} . (C) Sr contents show a negative correlation with strontium isotopes. (D) Mn contents show a positive correlation with strontium isotopes in vuggy dolostone samples. Sample symbols are as follows: diamond of blue filling for vuggy dolostones, diamond of yellow filling for crystalline dolostones, brown triangle for dolograinstones, blue rectangle for bioclastic limestones, and gray circle for marl limestones.

$\times 10^{-6}$) and 205×10^{-6} to 889×10^{-6} of Sr (mean value of 395×10^{-6}) and 85×10^{-6} to 771×10^{-6} of Mn (mean value of 369×10^{-6}) and 488×10^{-6} to $2,315 \times 10^{-6}$ of Sr (mean value of $1,366 \times 10^{-6}$), respectively. Correspondingly, the calculated Mn/Sr ratios of vuggy dolostones and other carbonates (i.e., marl limestones, bioclastic limestones, crystalline dolostones, and dolograinstones) displayed distinctively different values, ranging from 1.36 to 5.41 with a mean value of 3.51 and from 0.05 to 0.99 with a mean value of 0.30, respectively (Supplementary Table S2; Figure 4A). The concentration of Rb from all studied samples ranged from 0.01×10^{-6} to 0.08×10^{-6} with a mean value of 0.04×10^{-6} , generally less than 0.1 (Supplementary Table S2; Figure 4B). The carbonates displayed an Mn-increase–Sr-decrease trend with increasing dolomite components (Figure 5).

4.3 Radiogenic and stable isotopic characteristics

4.3.1 Strontium isotopes ($^{87}\text{Sr}/^{86}\text{Sr}$)

The $^{87}\text{Sr}/^{86}\text{Sr}$ values were measured for vuggy dolostones, dolograinstones, crystalline dolostones, and bulk limestones. For

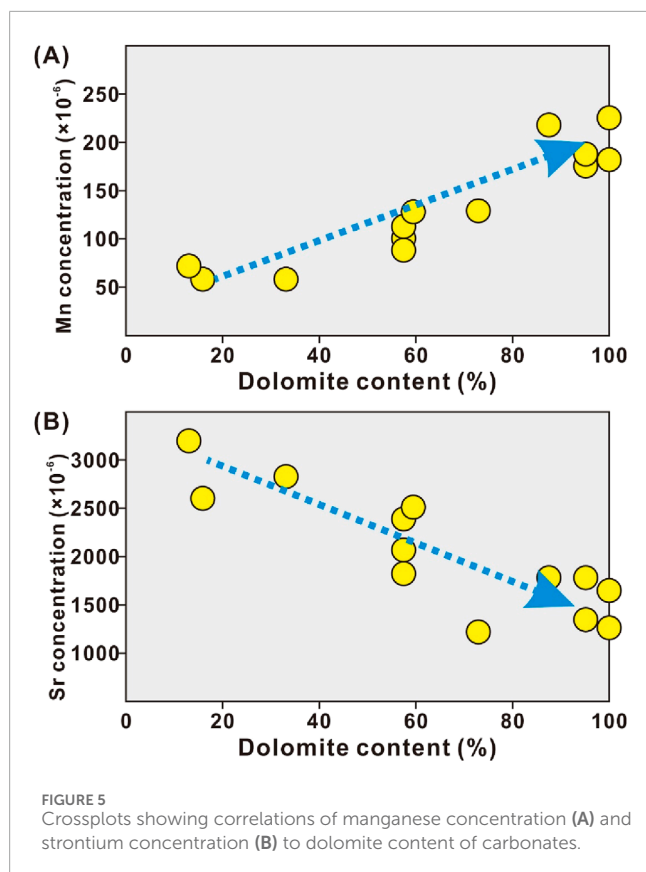
vuggy bioclastic dolograinstones, the $^{87}\text{Sr}/^{86}\text{Sr}$ ratios ranged from 0.708785 to 0.709411 with a mean value of 0.709125. By contrast, bioclastic/crystalline dolostone and limestone samples displayed lower strontium isotope composition, ranging from 0.707946 to 0.708523 with a mean value of 0.708160 (Supplementary Table S3; Figures 3, 4C).

4.3.2 Magnesium isotopes ($\delta^{26}\text{Mg}$)

The $\delta^{26}\text{Mg}$ composition was measured for crystalline dolostones and dolograinstones. At micritic dolostone–dolograinstone succession from the studied section, the $\delta^{26}\text{Mg}$ values ranged from -2.54‰ to -1.58‰ with a mean value of -2.09‰ and displayed an increasing trend with increasing depths (Supplementary Table S4; Figure 6). At medium-/coarse-sized to fine-sized crystalline dolostone succession from the studied interval, the $\delta^{26}\text{Mg}$ values ranged from -2.40‰ to -1.75‰ with a mean value of -2.09‰ and displayed a decreasing trend with increasing depths (Supplementary Table S4; Figure 7).

4.3.3 Carbon and oxygen isotopes ($\delta^{13}\text{C}$ and $\delta^{18}\text{O}$)

The $\delta^{13}\text{C}$ and $\delta^{18}\text{O}$ were measured for crystalline dolostones, dolograinstones, and bulk limestones. At micritic dolostone–bulk



limestone succession from the studied section, the $\delta^{13}\text{C}$ and $\delta^{18}\text{O}$ values ranged from -15.01‰ to -7.56‰ (mean value of -11.33‰) and -13.31‰ to -5.86‰ (mean value of -8.64‰), respectively (Supplementary Table S5; Figure 6). At the bulk limestone–crystalline dolostone succession from the studied interval, the $\delta^{13}\text{C}$ and $\delta^{18}\text{O}$ values ranged from 0.23‰ to 2.48‰ (mean value of 1.27‰) and -10.98‰ to -6.01‰ (mean value of -8.18‰), respectively (Supplementary Table S5; Figure 7).

4.4 Microthermometric characteristics

Homogenization temperatures of 24 fluid-inclusions from dolograinstones and 37 fluid-inclusions from crystalline dolostones range from 32°C to 66°C (mean value of 47°C) and 72°C – 136°C (mean value of 112°C), respectively (Figure 8).

5 Discussion

5.1 Validity assessment of seawater proxy

The representativeness of geochemical signatures of carbonates to coeval seawater should be evaluated (Liu et al., 2017; 2023). The diagenesis of marine carbonates is a process of Mn accumulation and Sr depletion. Hence, the Mn/Sr value is widely used to determine diagenetic alterations in carbonate rocks (Brand and Veizer, 1980; Huang, 1990; Huang et al., 2008). It is generally

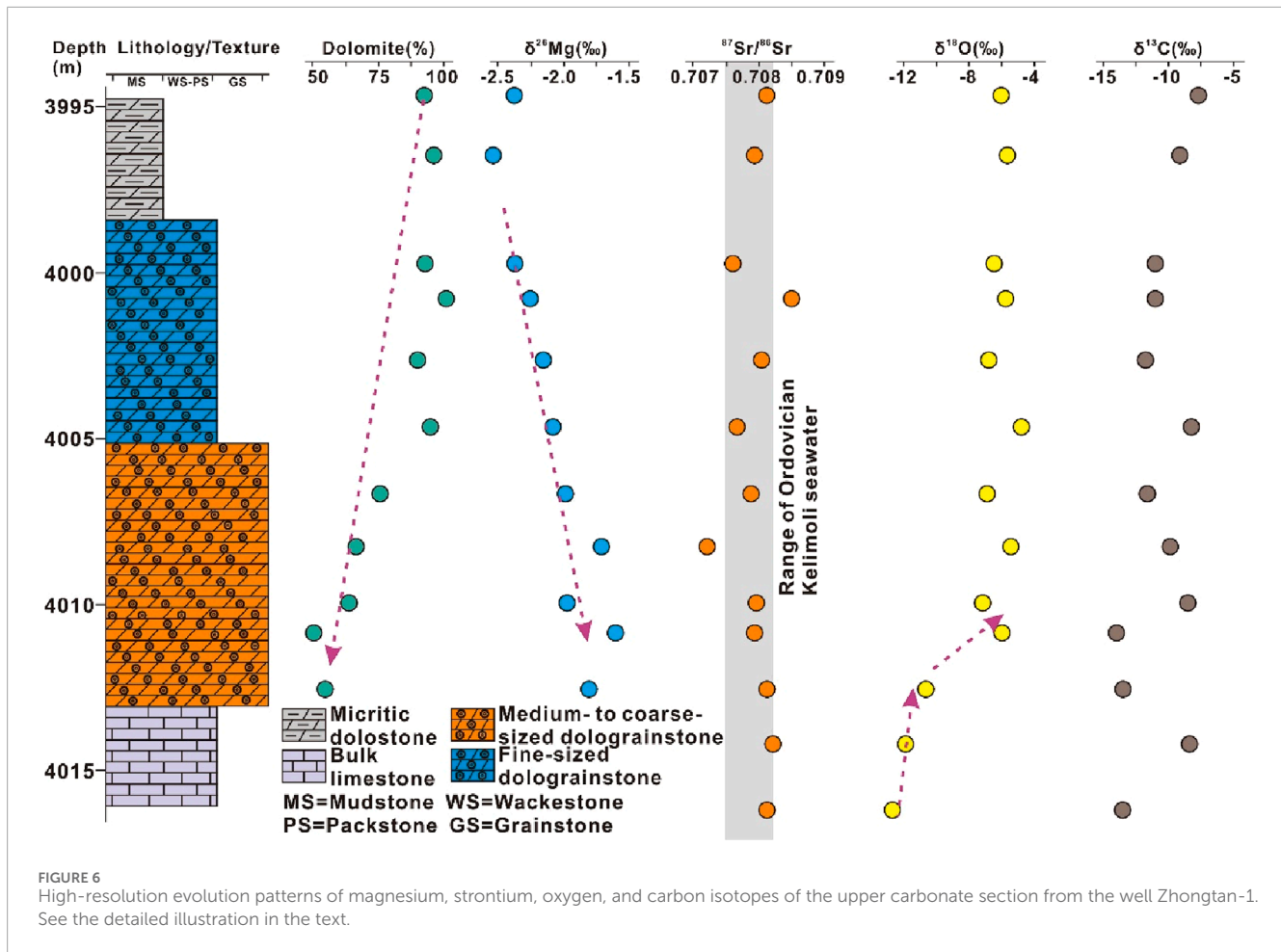
considered that the marine carbonates experience weak diagenetic alterations and inherit geochemical signatures of contemporaneous seawater when Mn/Sr ratios are less than 2 (Brand and Veizer, 1980). The micrites, bulk limestones, dolograinstones, and crystalline dolostones displayed very low Mn/Sr ratios with a mean value of ~ 0.30 , indicating that these carbonates inherited geochemical signatures of coeval seawater (Figure 4A). By contrast, the vuggy dolomites exhibit high Mn/Sr ratios with a mean value of 3.51, revealing that the original geochemical signatures of these dolomites were altered during the diagenetic process (i.e., meteoric leaching).

Rubidium influx should be evaluated because very less of rubidium (i.e., greater than 0.1×10^{-6}) during precipitation or diagenesis would cause significant deviation in the $^{87}\text{Sr}/^{86}\text{Sr}$ composition in marine carbonates due to radiogenic ^{87}Rb decaying into ^{86}Sr (Waight et al., 2002; Ramos et al., 2003). All dolomite samples were of low Rb concentrations with a mean value of 0.02×10^{-6} (Figure 4B), revealing that the strontium isotopes of carbonate samples were limitedly influenced by ^{87}Rb decaying.

The vuggy dolomites showed pronouncedly higher $^{87}\text{Sr}/^{86}\text{Sr}$ values than other types (Figures 3, 4C), reflecting terrestrial strontium influx with a high content of radiogenic strontium (i.e., ^{87}Sr) was involved (Saltzman et al., 2014; Sano et al., 2014). Meanwhile, the manganese concentration of meteoric water is much higher than that of seawater (Popp et al., 1986; Driese and Mora, 1993). The vuggy dolomites showed increasing $^{87}\text{Sr}/^{86}\text{Sr}$ values with increasing manganese contents, reflecting that the signature of meteoric water was inherited by these dolomites (Figure 4D). Collectively, dolomites and calcites being not influenced by meteoric water from the studied interval were valid proxy for geochemical signatures of coeval seawater, whereas dolomites experiencing meteoric leaching were geochemically modified.

5.2 Dolomite occurrence: meteoric water involved or not?

In previous studies, it was widely recognized that the Ordovician dolomites in the western Ordos basin was formed with involvement of meteoric water during shallow-burial diagenesis. This inference was mainly based on pronouncedly positive excursions of strontium compositions in dolostones developing dissolution macropores (Wang et al., 2009; He et al., 2014). Litho-/petro-facies evidence revealed that the dolomitization of Ordovician carbonates in the western Ordos basin occurred at a transition from marine environment to later-stage diagenetic fluids. Hence, the meteoric water–seawater mixing was widely recommended as a dolomitizing mechanism for Ordovician dolomites in the western Ordos basin (He et al., 2014). Nonetheless, the evidence from the current study did not support this declaration. First, dolograinstones, crystalline dolostones, and micrites that were spatially associated with dolostones experiencing meteoric leaching exhibited extremely low Fe and Mn concentrations. Particularly, these dolomites displayed similar Sr-isotopic composition to coeval Ordovician seawater. By contrast, vuggy dolostones showed pronouncedly higher $^{87}\text{Sr}/^{86}\text{Sr}$ values and Mn/Sr ratios than the above dolostone types (Figures 3, 4), revealing that this abnormal geochemical



signature was the result of alteration by meteoric water leaching after formation of dolomites. It is noteworthy that the Mn concentrations increased with increase in dolomite contents (i.e., evolving from limestones to dolostones, Figure 4D). However, this evolving trend was probably due to Mn accumulation during the dolomitizing process (Huang et al., 2008), but not related to meteoric water involvement. Moreover, the Mn contents of dolograins and crystalline dolomites were still much lower than that of dissolved dolostones (Figure 3). Second, the percentage of meteoric water that was required to form present Sr-isotopic composition in crystalline dolostones can be determined by quantitative calculation using the equations proposed by Stein et al. (2000):

$$\delta_L = (\delta_{sw} \cdot Sr_{sw} \cdot (1 - f_m) + \delta_m \cdot Sr_m \cdot f_m) / (Sr_{sw} \cdot (1 - f_m) + Sr_m \cdot f_m),$$

or,

$$f_m = ((\delta_{sw} - \delta_L) \cdot Sr_{sw}) / ((\delta_{sw} - \delta_L) \cdot Sr_{sw} + (\delta_L - \delta_m) Sr_m).$$

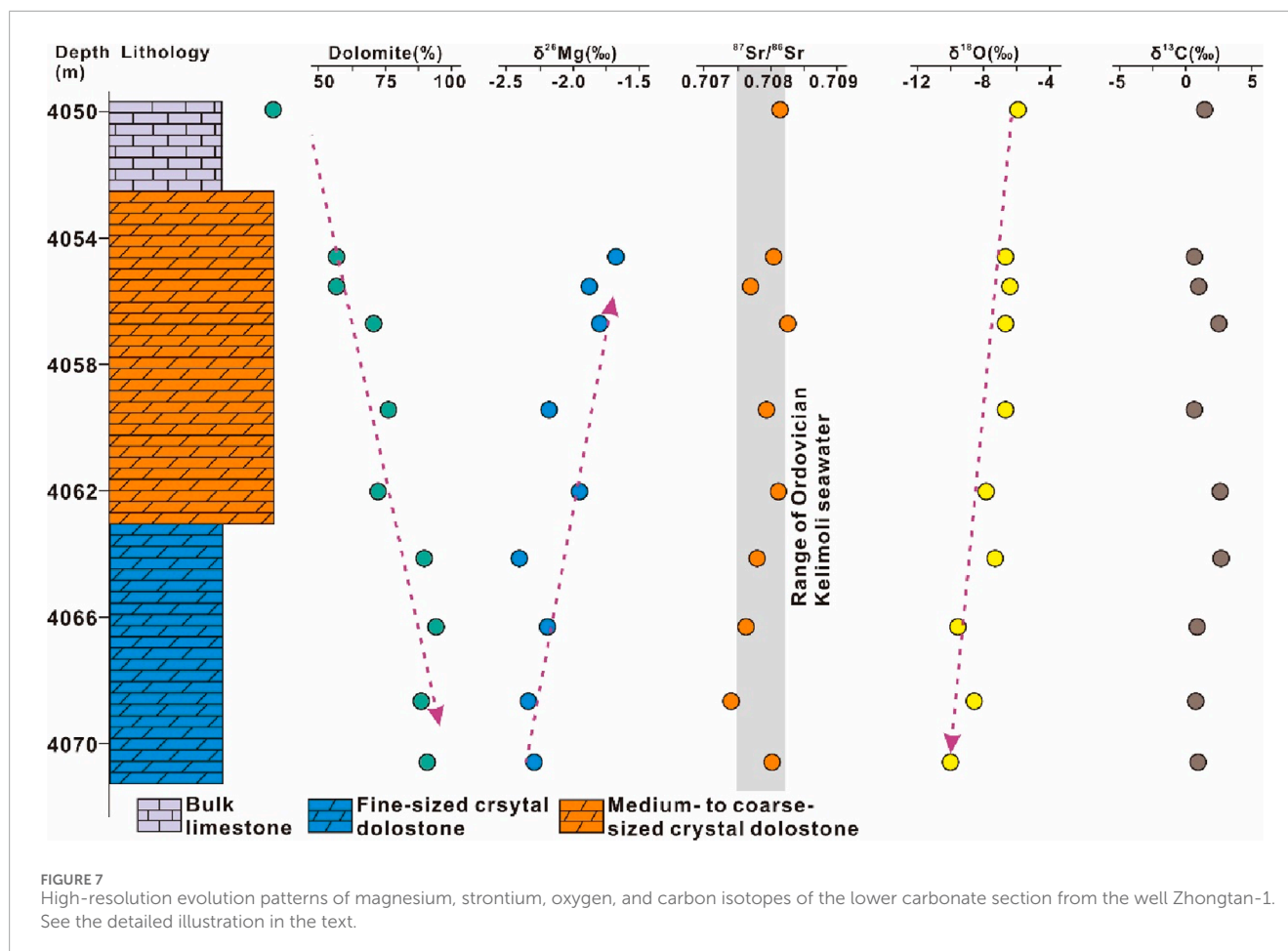
In equations, the Sr contents are expressed in mole concentrations, “f” for volume percentage, “δ” for Sr isotope composition (i.e., ⁸⁷Sr/⁸⁶Sr ratio), subscript “L” for dolomitizing fluid after marine-meteoric water mixing, “sw” for seawater, and “m” for meteoric water.

The mean value of Sr-isotopic composition of the Middle Ordovician is 0.708973 (Veizer et al., 1999), i.e., δ_{sw} = 0.708973.

The Sr-isotopic composition of the crystalline dolostones and dolograins represented that of dolomitizing fluid because these dolostones experienced limited diagenetic alterations, i.e., δ_L = 0.708160 (Supplementary Table S3; Figure 3). The Sr-isotopic composition of modern riverine water of a mean value of 0.711900 can be used as the strontium isotope of the meteoric water, i.e., δ_m = 0.711900 (Palmer and Edmond, 1989). The mean strontium contents of modern meteoric water (0.001 mmol/L; Livingstone, 1963) and marine water (0.097 mmol/L; Koepnick et al., 1985) can be used as Sr concentrations of the Ordovician Kelimoli meteoric and seawater water, i.e., Sr_{sw} = 0.097 mmol/L and Sr_m = 0.001 mmol/L, respectively.

Consequently, the calculated value of f_m is 0.96, indicating that referred dolomitization occurred in a type of mixture fluid composed by 96% of meteoric water and 4% of seawater. Theoretically, dolomitization would occur under this water-rock condition (Badiozamani, 1973). However, such high contents of terrestrial input should cause universal high Fe and Mn concentrations and ⁸⁷Sr/⁸⁶Sr ratios. However, it was not in line with geochemical features of Kelimoli dolostones.

In addition, the formation temperature of dolomites ranged from 40°C to 140°C according to fluid-inclusion microthermometry (Figure 8). Hence, the dolomites were formed at a depth of at least 600 m assuming that the near-surface temperature



was 25°C with a geothermal gradient of 25 °C/km. Evidently, mixing of riverine water and seawater could not occur at this burial depth. Hence, the formation of Kelimoli dolomites from the studied section had no connection with meteoric water.

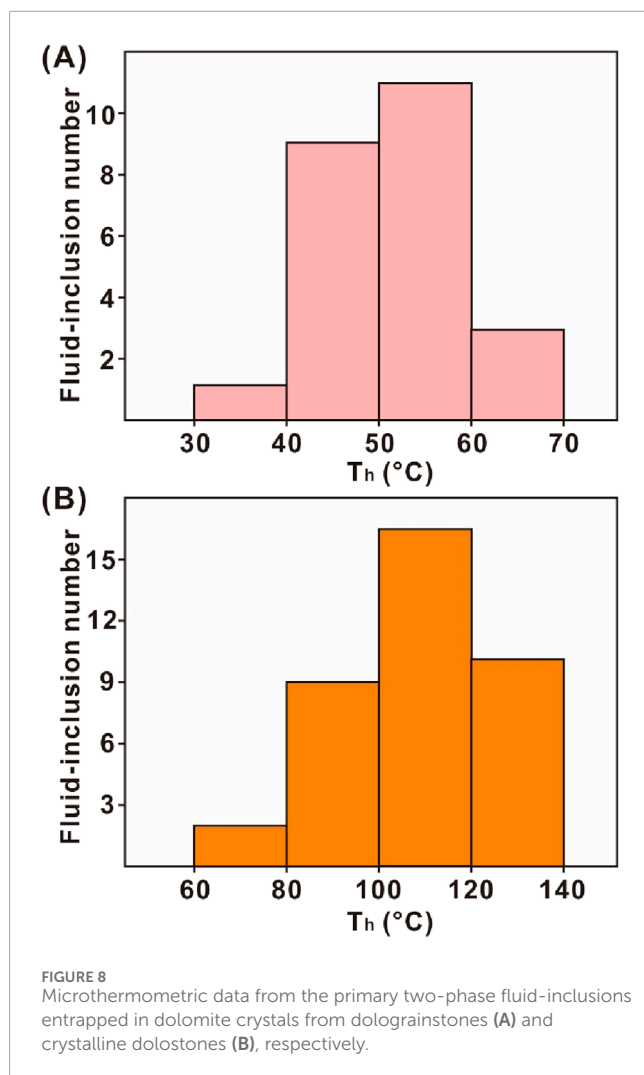
5.3 Origin and occurrence of dolomites

5.3.1 Evaporite–dolograinstone successions

The magnesium isotopy ($\delta^{26}\text{Mg}$) has important implications for deciphering the migration of dolomitizing fluids because $\delta^{26}\text{Mg}$ varies alongside flow pathways of dolomitizing fluids because light Mg (i.e., ^{24}Mg) is preferentially incorporated to form dolomites (Bialik et al., 2018; Li et al., 2019). Two evolution types of Mg-isotopic composition were determined from the studied sections. The first type was characterized by $\delta^{26}\text{Mg}$ increasing downwardly with carbonate successions of topmost micritic dolostones, upper fine-sized dolograins, lower medium- to coarse-sized dolograins, and bottom bulk limestones. Meanwhile, dolomite content decreased gradually from topmost micrites to bottom limestones (Figure 6). Probably, the dolomitizing fluid migrated downward to dolomitize limestones. In this carbonate succession, the upper section displayed bioclastic texture and high dolomite content. By contrast, the lower section developed coarse-sized

crystals characterized by mosaic contact and cloudy-cores–clear-rims texture (Figure 2E), indicating that these dolomites precipitated directly from dolomitizing fluid at a later stage. Studied dolostones inherited Sr-isotopic composition of coeval Ordovician Kelimoli seawater, except those developing vuggy pores (Figure 6). The $\delta^{18}\text{O}$ values displayed a positive excursion against a long-term decreasing background, revealing that the oxygen isotope depletion caused by burial recrystallization was buffered by meteoric leaching at a certain extent (Eren et al., 2007; Liu et al., 2016). Different from strontium and oxygen isotopes, the carbon isotopes ($\delta^{13}\text{C}$) exhibited stable values at the studied interval, reflecting that meteoric leaching did not alter the carbon isotopic composition of dolomites (Figure 6). Meanwhile, depleted $\delta^{13}\text{C}$ values indicated that the carbon probably originated from marine organisms because light carbon, i.e., ^{12}C , was preferentially absorbed by organisms (Meyer et al., 2011; Liu et al., 2023). This inference was consistent with lithologic features of dolograins, i.e., developing abundant bioclastics and organic remnant fossils (Figure 2D). Therefore, the above evidence revealed that the dolomitizing fluid was sourced from marine water (seawater or relevant brine water). Otherwise, it should display different strontium and carbon isotopic compositions.

Combined with the microthermometric result (i.e., formation temperature of dolograins of ~47°C), it can be concluded



that the dolograinsstones from the studied section were the result of seepage reflux and burial dolomitization. This declaration was also supported by previous lithofacies and geochemical studies (Wang et al., 2009; He et al., 2014).

5.3.2 Crystalline dolostone successions

Another type of $\delta^{26}\text{Mg}$ evolution and dolomite content showed a decreasing trend (Figure 7), revealing that the dolomitizing fluid migrated upwardly from the studied section. This evolving trend occurred in the carbonate successions of topmost bulk limestones, upper coarse-sized, and lower fine-sized crystalline dolostones. Mosaic contact and planar-e of dolomite crystals indicated that the dolomites from the studied section were precipitated from dolomitizing fluid directly under a low water-rock ratio (Figures 2F, G; Eren et al., 2007). Hence, the dolomitizing process was consistent with the “diffusion model” concluded by Huang et al. (2015). At the onset of the dolomitizing process, dolomites were precipitated at a high rate with high head pressure and flow rate, thus forming fine-sized dolomite crystals. Meanwhile, light magnesium (i.e., ^{24}Mg) was preferentially incorporated during dolomite precipitation. As the dolomitizing fluid migrated

upwardly, the flow rate of the dolomitizing fluid was slackened gradually, thus forming coarse-sized dolomite crystals and rich in ^{26}Mg because of ^{24}Mg consumption. The $^{87}\text{Sr}/^{86}\text{Sr}$ ratios were in line with Sr-isotopic composition of coeval Ordovician seawater. Meanwhile, the fluid-inclusion microthermometry indicated that crystalline dolomites were formed at the temperature of 72°C – 136°C (Figure 8B). Hence, the dolomitizing fluid was derived from sealed brine water that was intimately associated with coeval seawater. The oxygen isotopic composition showed slight negative excursion downwardly, probably reflecting recrystallization with increasing burial depth. Compared with dolograinsstones, the carbon isotopic composition was rich in ^{13}C (Figures 6, 7), revealing that the carbon was derived from inorganic origin and precipitated from coeval seawater directly (Meyer et al., 2011; Song et al., 2012; Liu et al., 2023). To conclude, the crystalline dolostone succession was formed due to burial dolomitization.

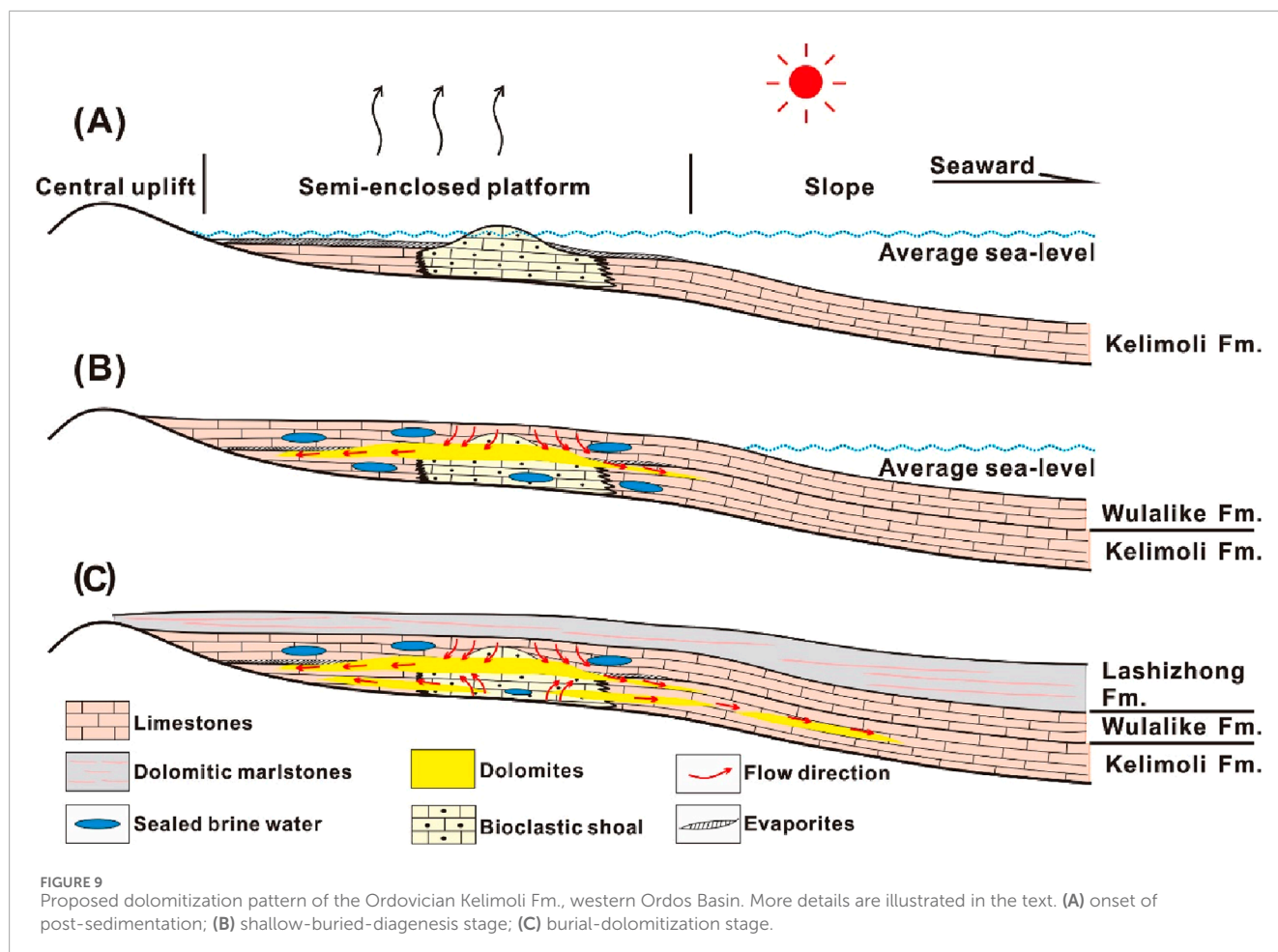
5.4 Dolomitization pattern

Based on the previous discussion, the dolomitization pattern from the studied section can be concluded as following stages (Figure 9). At the onset of post-sedimentation of the Kelimoli Fm. (i.e., the first stage), the open tidal flat was closed due to the development of platform shoals (He et al., 2014). Intensive evaporation caused by arid climate, coupled with magnesium ions supplying from restricted-circulation seawater, promoted the precipitation of evaporative dolomites (Figure 9A). During shallow-buried diagenesis (i.e., the second stage), the seawater-sourced fluids rich in magnesium ions seeped downwardly and migrated laterally to dolomitize limestones (Figure 9B). Meanwhile, some seawater-sourced fluid was sealed as brine water. With increasing burial depths, the sealed brine water was released under high pressure and migrated upwardly and laterally along high-porosity conduits, thereby dolomitizing the surrounding limestones (Figure 9C). The strontium contents increased from crystallized dolomites to clastic calcites in lateral-contact successions. This geochemical feature corresponded to the weakened dolomitizing process laterally. Fine-sized dolomites commonly had large initial porosities, thus providing preferential flowing conduits for dolomitization. With progressive intrusion of brine water into lateral limestones, the dolomitizing process was slackened due to low porosities of limestones and low fluid-rock ratios (Peng et al., 2016), thus forming coarse-sized crystallized dolomites. Meanwhile, the occurrence of sporadic porphyritic dolomites indicated the end of dolomitizing fluid in tight bulk limestones (Qiao et al., 2023).

6 Conclusion

Based on the current study, the following conclusions can be drawn.

- (1) Carbonates experiencing no meteoric leaching from the studied section inherited geochemical signatures of coeval



seawater faithfully, thus providing effective proxies for ancient seawater. By contrast, vuggy dolostones underwent meteoric leaching modifications and were geochemically altered from coeval seawater.

- The discussed dolostones experiencing no meteoric leaching (i.e., crystalline dolostones, dolograinstones, and micritic dolostones) exhibited low concentrations of Fe and Mn exclusively. Meanwhile, the strontium isotopic composition of these dolostones was consistent with that of coeval seawater. Hence, the formation of dolomites predated the meteoric leaching and meteoric water was not involved in dolomitization. Moreover, quantitative calculation of strontium composition revealed that at ~ 96% of meteoric water was required for occurrence of meteoric seawater-mixing dolomitization. In addition, microthermometry indicated that the dolomitization occurred at a deep-burial and high-temperature environment, at which massive meteoric water involvement could not occur.
- $\delta^{26}\text{Mg}$ can be an important indicator for migration of dolomitizing fluids. Comprehensive $\delta^{26}\text{Mg}$, $^{87}\text{Sr}/^{86}\text{Sr}$, $\delta^{13}\text{C}$, and $\delta^{18}\text{O}$ isotopes revealed that reservoir dolostones of the studied section (i.e., micritic dolostones being not included) were formed at a burial environment. At the first stage

(i.e., a shallow-burial stage), the dolomitizing fluid composed by syn-depositional seawater migrated downwardly, forming dolograinstones. At the second stage (i.e., a deep-burial stage), the dolomitizing fluid derived from sealed brine water moved upwardly, forming crystalline dolostones. The two types of dolostones constituted potential hydrocarbon reservoir rocks.

Data availability statement

The original contributions presented in the study are included in the article/Supplementary Material; further inquiries can be directed to the corresponding author.

Author contributions

XJ: writing–original draft and writing–review and editing. JT: data curation and writing–review and editing. LZ: funding acquisition, supervision, validation, and writing–review and editing. FL: methodology, visualization, and writing–review and editing. HL: formal analysis, investigation, software, and writing–review and editing.

Funding

The author(s) declare that financial support was received for the research, authorship, and/or publication of this article. The current study is funded by major science and technology project of PetroChina Changqing Oilfield Company, “Comprehensive Interpretation and Basic Geological Research of Ordos Basin Seismic Framework and Large Section” (Grant No. 2023DZZ02). The funder was not involved in the study design, collection, analysis, interpretation of data, the writing of this article, or the decision to submit it for publication.

Conflict of interest

Authors XJ, LZ, and HL were employed by Exploration and Development Research Institute of Changqing Oilfield Company, PetroChina.

The remaining authors declare that the research was conducted in the absence of any commercial or financial relationships that could be construed as a potential conflict of interest.

References

- Ali, J., Ashraf, U., Anees, A., Peng, S., Umar, M., Thanh, H., et al. (2022). Hydrocarbon potential assessment of carbonate-bearing sediments in a meyal oil field, Pakistan: insights from logging data using machine learning and quanti elan modeling. *ACS Omega* 7 (43), 39375–39395. doi:10.1021/acsomega.2c05759
- Amthor, J. E., Mountjoy, E. W., and Machel, H. G. (1993). Subsurface dolomites in Upper Devonian Leduc Formation buildups, central part of rimbey-meadowbrook reef trend, Alberta, Canada. *Bull. Can. Petroleum Geol.* 41 (2), 164–185.
- Ashraf, U., Zhang, H., Anees, A., Ali, M., Mangi, H., and Zhang, X. (2024a). An ensemble-based strategy for robust predictive volcanic rock typing efficiency on a global-scale: a novel workflow driven by big data analytics. *Sci. Total Environ.* 937, 173425. doi:10.1016/j.scitotenv.2024.173425
- Ashraf, U., Zhang, H., Anees, A., Zhang, X., and Duan, L. (2024b). Assessment of lake-level variations to decipher geological controlling factors and depositional architecture of Lake Fuxian, Yunnan Plateau: preliminary insights from geophysical data. *Geomech. Geophys. Geo* 10, 64. doi:10.1007/s40948-024-00777-7
- Azomani, E., Azmy, K., Blamey, N., Brand, U., and Al-Aasm, I. (2013). Origin of Lower Ordovician dolomites in Eastern Laurentia: controls on porosity and implications from geochemistry. *Mar. Petr. Geol.* 40 (1), 99–114. doi:10.1016/j.marpetgeo.2012.10.007
- Badiozamani, K. (1973). The dorag dolomitization model application to the middle Ordovician of Wisconsin. *J. Sediment. Petrol.* 43 (4), 965–984.
- Bialik, O. M., Wang, X. M., Zhao, S. G., Waldmann, N. D., Frank, R., and Li, W. Q. (2018). Mg isotope response to dolomitization in hinterland attached carbonate platforms: outlook of $\delta^{26}\text{Mg}$ as a tracer of basin restriction and seawater Mg/Ca ratio. *Geochim. Cosmochim. Acta* 235, 189–207. doi:10.1016/j.gca.2018.05.024
- Brand, U., and Veizer, J. (1980). Chemical diagenesis of multicomponent carbonate system-1: trace elements. *J. Sediment. Petrol.* 50, 1219–1236.
- Davies, G. R., and Smith, L. B. (2006). Structurally controlled hydrothermal dolomite reservoir facies: an overview. *AAPG Bull.* 90 (11), 1641–1690. doi:10.1306/05220605164
- Dickson, J. A. D. (1965). A modified staining technique for carbonates in thin section. *Nature* 205, 587. doi:10.1038/205587a0
- Driese, S. G., and Mora, C. (1993). Physico-chemical environment of pedogenic carbonate formation in Devonian vertic palaeosols, central Appalachians, USA. *Sedimentology* 40 (2), 199–216. doi:10.1111/j.1365-3091.1993.tb01761.x
- Eren, M., Kaplan, M. Y., and Kadir, S. (2007). Petrography, geochemistry and origin of Lower Liassic dolomites in the Aydinçik area, Mersin, southern Turkey. *Turk. J. Earth Sci.* 16 (3), 339–362.
- Fan, B. (2022). Geochemical characteristics and paleoenvironment of organic-rich triassic shale in the central Ordos Basin. *Nat. Resour. Res.* 31 (3), 1739–1757. doi:10.1007/s11053-022-10068-1
- He, X., Shou, J., Shen, A., Wu, X., Wang, Y., Hu, Y., et al. (2014). Geochemical characteristics and origin of dolomite: a case study from the middle assemblage of

Generative AI statement

The authors declare that no Generative AI was used in the creation of this manuscript.

Publisher's note

All claims expressed in this article are solely those of the authors and do not necessarily represent those of their affiliated organizations, or those of the publisher, the editors and the reviewers. Any product that may be evaluated in this article, or claim that may be made by its manufacturer, is not guaranteed or endorsed by the publisher.

Supplementary material

The Supplementary Material for this article can be found online at: <https://www.frontiersin.org/articles/10.3389/feart.2025.1563155/full#supplementary-material>

majiagou formation member 5 of the west of jingbian gas field, Ordos Basin, north China. *Petrol. Explor. Dev.* 41 (3), 375–384.

Higgins, J. A., Blattler, C. L., Lundstrom, E. A., Santiago-Ramos, D. P., Akhtar, A. A., Cruger-Ahm, A. S., et al. (2018). Mineralogy, early marine diagenesis, and the chemistry of shallow-water carbonate sediments. *Geochim. Cosmochim. Acta* 220, 512–534. doi:10.1016/j.gca.2017.09.046

Hou, F., Fang, S., Dong, Z., Zhao, J., Lu, S., Wu, Y., et al. (2003). The developmental characters of sedimentary environments and lithofacies of middle Ordovician Majiagou Formation in Ordos Basin. *Acta Sedimentol. Sini.* 21 (1), 106–112.

Hu, T., Jiang, F., Pang, X., Liu, Y., Wu, G., Zhou, K., et al. (2024a). Identification and evaluation of shale oil micro-migration and its petroleum geological significance. *Petrol. Explor. Dev.* 51 (1), 127–140. doi:10.1016/s1876-3804(24)60010-8

Hu, T., Jing, Z., Zhang, Q., Pan, Y., Yuan, M., and Li, Y. (2025). Shale oil micro-migration characterization: key methods and outlook. *Adv. Geo. Res.* 15 (1), 5–12. doi:10.46690/ager.2025.01.02

Hu, T., Liu, Y., Jiang, F., Pang, X., Wang, Q., Zhou, K., et al. (2024b). A novel method for quantifying hydrocarbon micromigration in heterogeneous shale and the controlling mechanism. *Energy* 288, 129712. doi:10.1016/j.energy.2023.129712

Huang, K., Shen, B., Lang, X., Tang, W., Peng, Y., Ke, S., et al. (2015). Magnesium isotopic compositions of the Mesoproterozoic dolostones: implications for Mg isotopic systematics of marine carbonates. *Geochim. Cosmochim. Acta* 164, 333–351. doi:10.1016/j.gca.2015.05.002

Huang, S. (1990). Cathodoluminescence and diagenetic alternation of marine carbonate minerals. *Sediment. Geol. Teth. Geol.* 10 (4), 9–15.

Huang, S. J., Qing, H. R., Huang, P. P., Hu, Z. W., Wang, Q. D., Zou, M. L., et al. (2008). Evolution of strontium isotopic composition of seawater from Late Permian to Early Triassic based on study of marine carbonates, Zhongliang Mountain, Chongqing, China. *Sci. Ch.-Earth Sci.* 51 (4), 528–539. doi:10.1007/s11430-008-0034-3

Imai, N., Terashima, S., Itoh, S., and Ando, A. (1996). 1996 Compilation of analytical data on nine GSJ geochemical reference samples, “sedimentary rock series”. *Geostand. Newsl.* 20, 165–216. doi:10.1111/j.1751-908X.1996.tb00184.x

Kimmig, S. R., Nadeau, M. D., Swart, P. K., and Holmden, C. (2021). Mg and Sr isotopic evidence for basin wide alteration of early diagenetic dolomite in the Williston Basin by ascending crustal fluids. *Geochim. Cosmochim. Acta* 311, 198–225. doi:10.1016/j.gca.2021.06.006

Koepnick, R. B., Burke, W. H., Denison, R. E., Hetherington, E. A., Nelson, H. F., Otto, J. B., et al. (1985). Construction of the seawater curve for the cenozoic and cretaceous: supporting data. *Chem. Geol. Isot. Geosci.* 58 (1), 55–81. doi:10.1016/0168-9622(85)90027-2

Li, M. (2019). Analysis of sedimentary and tectonic evolution of the western margin of Ordos area in Ordovician. Doctoral Dissertation. Evanston: Northwestern University.

- Li, W., Bialik, O. M., Wang, X., Yang, T., Hu, Z., Huang, Q., et al. (2019). Effects of early diagenesis on Mg isotopes in dolomite: the roles of Mn (IV)-reduction and recrystallization. *Geochim. Cosmochim. Acta* 250, 1–17. doi:10.1016/j.gca.2019.01.029
- Liu, C., Jiang, T., Yang, Y., and Ma, J. (2023). Temporal and spatial variations of high-resolution strontium, carbon, and oxygen isotopic chemostratigraphy at the end-Permian crisis boundary in South China. *Gondwana Res.* 113, 89–101. doi:10.1016/j.gr.2022.10.015
- Liu, C., Xie, Q., Wang, G., He, W., Song, Y., Tang, Y., et al. (2017). Rare earth element characteristics of the Carboniferous Huanglong formation dolomites in eastern Sichuan Basin, southwest China: implications for origins of dolomitizing and diagenetic fluids. *Mar. Pet. Geol.* 81, 33–49. doi:10.1016/j.marpetgeo.2016.12.030
- Liu, C., Xie, Q., Wang, G., Song, Y., and Qi, K. (2016). Dolomite origin and its implication for porosity development of the carbonate gas reservoirs in the Upper Permian Changxing Formation of the eastern Sichuan Basin, Southwest China. *J. Nat. Gas. Sci. Eng.* 35, 775–797. doi:10.1016/j.jngse.2016.09.027
- Livingstone, D. A. (1963). Chemical composition of rivers and lakes. *Data of Geochemistry*. Editor M. Fleischer, 41–44.
- Meyer, K. M., Yu, M., Jost, A. B., Kelley, B. M., and Payne, J. L. (2011). $\delta^{13}\text{C}$ evidence that high primary productivity delayed recovery from end-Permian mass extinction. *Earth Planet. Sci. Lett.* 302, 378–384. doi:10.1016/j.epsl.2010.12.033
- Murray, R. W., Gerlach, D. C., Iii, G. P. R., and Jones, D. L. (1991). Rare earth, major, and trace elements in chert from the Franciscan Complex and Monterey Group, California: assessing ree sources to fine-grained marine sediments. *Geochim. Cosmochim. Acta* 55 (7), 1875–1895. doi:10.1016/0016-7037(91)90030-9
- Ning, M., Lang, X., Huang, K., Li, C., Huang, T., Yuan, H., et al. (2020). Towards understanding the origin of massive dolostones. *Earth Planet. Sci. Lett.* 545, 116403. doi:10.1016/j.epsl.2020.116403
- Nothdurft, L. D., Webb, G. E., and Kamber, B. S. (2004). Rare earth element geochemistry of Late Devonian reefal carbonates, Canning Basin, Western Australia: confirmation of a seawater ree proxy in ancient limestones. *Geochim. Cosmochim. Acta* 68 (2), 263–283. doi:10.1016/s0016-7037(03)00422-8
- Palmer, M. R., and Edmond, J. M. (1989). The strontium isotope budget of the modern ocean. *Earth Planet. Sci. Lett.* 92 (1), 11–26. doi:10.1016/0012-821x(89)90017-4
- Peng, Y., Shen, B., Lang, X., Huang, K., Chen, J., Yan, Z., et al. (2016). Constraining dolomitization by mg isotopes: a case study from partially dolomitized limestones of the middle cambrian xuzhuang formation, North China. *Geochim. Geophys. Geosyst.* 17 (3), 1109–1129. doi:10.1002/2015gc006057
- Popp, B. N., Podosek, F. A., Brannon, J. C., Anderson, T. F., and Pier, J. (1986). $^{87}\text{Sr}/^{86}\text{Sr}$ ratios in Permo-Carboniferous seawater from the analyses of well-preserved brachiopod shells. *Geochim. Cosmochim. Acta* 50 (7), 1321–1328. doi:10.1016/0016-7037(86)90308-x
- Qiao, Z., Shen, A., Liang, F., Shao, G., Zhang, T., Luo, X., et al. (2023). Magnesium isotope-based forming process of large sized burial dolomite: a case study of the Penglaiba Formation in Tarim basin. *Acta Geol. Sini.* 97 (7), 2293–2310.
- Ramos, F. C., Wolff, J. A., and Tollstrup, D. L. (2003). Measuring $^{87}\text{Sr}/^{86}\text{Sr}$ variations in minerals and groundmass from basalts using LA-MC-ICPMS. *Chem. Geol.* 211, 135–158. doi:10.1016/j.chemgeo.2004.06.025
- Saltzman, M. R., Edwards, C. T., Leslie, S. A., Dwyer, G. S., Bauer, J. A., Repetski, J. E., et al. (2014). Calibration of a conodont apatite-based Ordovician $^{87}\text{Sr}/^{86}\text{Sr}$ curve to biostratigraphy and geochronology: implications for stratigraphic resolution. *GSA Bull.* 126 (11/12), 1551–1568. doi:10.1130/b31038.1
- Sano, Y., Toyoshima, K., Shirai, A., Komiya, T., Takahata, N., Sato, T., et al. (2014). Ion microprobe U-Pb dating and Sr isotope measurement of a protoconodont. *J. Asian Earth Sci.* 92, 10–17. doi:10.1016/j.jseas.2014.05.024
- Shepherd, T. J., Rankin, A. H., and Alderton, D. H. M. (1985). *A practical guide to fluid inclusion studies*. London: Blackie.
- Shields, G., and Stille, P. (2001). Diagenetic constraints on the use of cerium anomalies as palaeoseawater redox proxies: an isotopic and REE study of Cambrian phosphorites. *Chem. Geol.* 175 (1–2), 29–48. doi:10.1016/s0009-2541(00)00362-4
- Song, H., Tong, J., Xiong, Y., Sun, D., Li, T., and Song, H. (2012). The large increase of $\delta^{13}\text{C}$ carb-depth gradient and the end-Permian mass extinction. *Sci. Ch.-Earth Sci.* 55 (7), 1101–1109. doi:10.1007/s11430-012-4416-1
- Stein, M., Starinsky, A., Agnon, A., Katz, A., Raab, M., and Spiro, B. (2000). The impact of brine-rock interaction during marine evaporite formation on the isotopic Sr record in the oceans: evidence from Mt. Sedom, Israel. *Geochim. Cosmochim. Acta* 64 (12), 2039–2053.
- Su, Z., Hu, S., Liu, B., Ren, J., and Bai, H. (2016). Characteristics and controlling factors of paleokarst caves in Kelimoli Formation, west Ordos Basin, China. *J. Chengdu Univ. Technol.* 43 (2), 233–240.
- Veizer, J., Ala, D., Azmy, K., Bruckschen, K., Buhl, D., Bruhn, F., et al. (1999). $^{87}\text{Sr}/^{86}\text{Sr}$, $\delta^{13}\text{C}$ and $\delta^{18}\text{O}$ evolution of Phanerozoic seawater. *Chem. Geol.* 161 (30), 59–88. doi:10.1016/s0009-2541(99)00081-9
- Waight, T., Baker, J., and Peate, D. (2002). Sr isotope ratio measurements by double-focusing MC-ICP-MS: techniques observations and pitfalls. *Int. J. Mass. Spectrom.* 221, 229–244. doi:10.1016/s1387-3806(02)01016-3
- Wang, B., Qiang, Z., Zhang, F., Wang, X., Wang, Y., and Cao, W. (2009). Isotope characteristics of dolomite from the fifth member of the ordovician majiagou formation, the Ordos Basin. *Geochim. Acta* 73 (5), 472–479.
- Warren, J. (2000). Dolomite: occurrence, evolution and economically important associations. *Earth Sci. Rev.* 52 (1), 1–81. doi:10.1016/s0012-8252(00)00022-2
- Webb, G. E., and Kamber, B. S. (2000). Rare earth elements in Holocene reefal microbialites: a new shallow seawater proxy. *Geochim. Cosmochim. Acta* 64 (9), 1557–1565. doi:10.1016/s0016-7037(99)00400-7
- Webb, G. E., Nothdurft, L. D., Kamber, B. S., Klopogge, J. T., and Zhao, J. X. (2009). Rare earth element geochemistry of scleractinian coral skeleton during meteoric diagenesis: a sequence through neomorphism of aragonite to calcite. *Sedimentology* 56 (5), 1433–1463. doi:10.1111/j.1365-3091.2008.01041.x
- Wu, X., Wu, D., Ding, Z., Yu, Z., Wang, S., and Li, W. (2020). Geochemical characteristics and genetic analysis of Ordovician dolomites in the western margin of Ordos Basin. *Mar. Ori. Petrol. Geol.* 25 (4), 312–318.
- Yang, Y. H., Zhang, H. F., Wu, F. Y., Xie, L. W., and Zhang, Y. B. (2005). Accurate measurement of strontium isotopic composition by Neptune multiple-collector inductively coupled plasma mass spectrometry. *J. Chin. Mass. Spectr. Soc.* 26 (4), 215–221.
- Yu, Z., Zhou, J., Li, C., Song, X., Luo, C., Wu, X., et al. (2021). Tectonic-lithofacies paleogeographic characteristics of ordovician Kelimoli and Wulalike stages in the western edge of Ordos Basin. *Nat. Gas. Geosci.* 32 (6), 816–825.